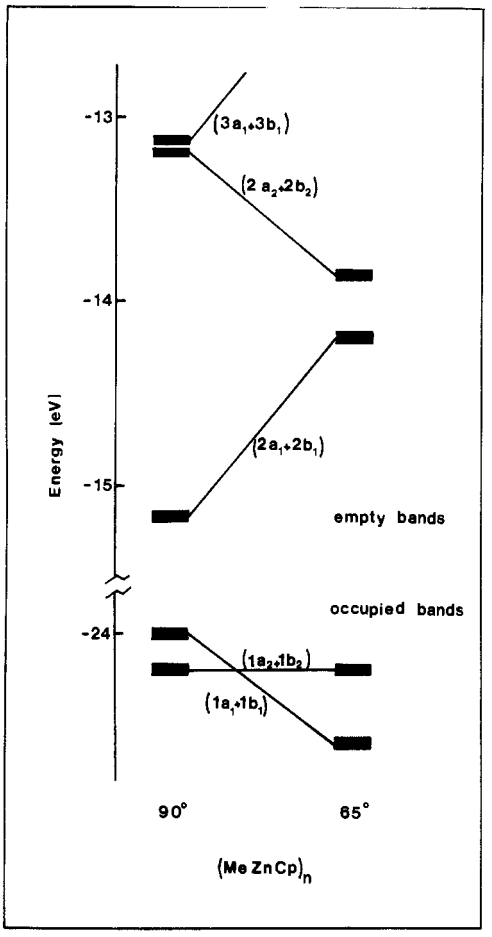

Figure 4. Solid-state Walsh diagram for the variation of θ from 90 to 65° in $(CH_3ZnCp)_n$.

in $(BC_4H_5)_2Pb$ should be inclined with respect to the Pb–Pb direction.

(3) More bands could be emptied by a systematic replacement of carbon by boron in the cyclopentadienyl ligands. Boron heterocycles are currently employed as bridging ligands in triple-decker or higher order systems.[15] Interesting electronic and magnetic properties may be expected. The electron count can be further tuned by changing the nature of the main-group metal center. An ample range of interesting polymeric systems can be envisaged on this basis.

Acknowledgment. We are grateful to Dr. S. D. Wijeyesekera for his help in adapting the band program and to Professor T. A. Albright for communication of results prior to publication. E.C. thanks the Department of Chemistry of the University of Michigan for their hospitality. O.E. acknowledges the donors of the Petroleum Research Fund, administered by the American Chemical Society, for support of this research.

Appendix

The exponents and parameters are given in Table I. The modified weighted Wolfsberg–Helmholtz formula was used.[16] The following structural parameters were used: Pb–center capping Cp = 2.486 Å, Pb–center bridging Cp = 2.818 Å, C–C(Cp) = 1.4095 Å, C(Cp)–H = 1.08 Å; Zn–C(CH_3) = 1.97 Å, C(CH_3)–H = 1.09 Å, Zn–center bridging Cp = 2.455 Å; Mn–center capping Cp = 2.095 Å; Mn–center bridging Cp = 2.69 Å; ∠Pb–Pb–Pb = 120°, ∠Zn–Zn–Zn = 148°, ∠Mn–Mn–Mn = 120°.

Registry No. $(Cp_2Pb)_n$, 90623-40-8; $(CH_3ZnCp)_n$, 90623-41-9; $(Cp_2Mn)_n$, 90623-42-0.

(15) Siebert, W. *Adv. Organomet. Chem.* **1980**, *18*, 301.
(16) Ammeter, J. H.; Bürgi, H.-B.; Thibeault, J. C.; Hoffmann, R. *J. Am. Chem. Soc.* **1978**, *100*, 3686.
(17) Summerville, R. H.; Hoffmann, R. *J. Am. Chem. Soc.* **1976**, *98*, 7240.
(18) Silvestre, J.; Albright, T. A. *Isr. J. Chem.* **1983**, *23*, 139.
(19) In fact, a minimum in the total energy is found for θ near 90°. If θ takes on larger values, the structure is destabilized by loss of bonding interactions in lower bands.

Contribution from the Department of Chemistry, Faculty of Science, Kyushu University, Higashiku, Fukuoka 812, Japan

Examples of Fast and Slow Electronic Relaxation between ^6A and ^2T

YONEZO MAEDA,* NAOTO TSUTSUMI, and YOSHIMASA TAKASHIMA

Received April 15, 1983

The iron(III) complexes $[Fe(sapa)_2]Y\cdot{}^3/_2H_2O$, $[Fe(vapa)_2]Y$, $[Fe(acpa)_2]Y\cdot H_2O$, and $[Fe(bzpa)_2]Y\cdot 2H_2O$ (Y = PF_6, BPh_4, NO_3) were synthesized, and the phenomenon of the spin transition between the low-spin ($S = {}^1/_2$) and high-spin ($S = {}^5/_2$) states depending on temperature was confirmed by the temperature-dependent magnetism and Mössbauer spectra. The tridentate ligands used here were *N*-salicylidene-2-pyridylmethylamine (Hsapa), *N*-(3-methoxysalicylidene)-2-pyridylmethylamine (Hvapa), *N*-(1-acetyl-2-propylidene)-2-pyridylmethylamine (Hacpa), and *N*-(1-benzoyl-2-propylidene)-2-pyridylmethylamine (Hbzpa). The "time-averaged" Mössbauer spectra between the low- and high-spin states were observed for $[Fe(acpa)_2]BPh_4\cdot H_2O$, $[Fe(bzpa)_2]PF_6\cdot 2H_2O$, and $[Fe(acpa)_2]NO_3\cdot H_2O$; the relaxation time of the change from the high-spin to the low-spin state (and vice versa) is faster than the ^{57}Fe Mössbauer lifetime (1×10^{-7} s). The activation energy for the spin-interchange crossing was calculated to be 2.4 kcal/mol for solid $[Fe(acpa)_2]BPh_4\cdot H_2O$. The results are interpreted in terms of a model in which the spin-interchange crossing is treated as an intramolecular mechanism, internal electron-transfer reaction. The ground-state Kramers doublet in the $[Fe(acpa)_2]^+$ series has one unpaired electron in a d_{xy} orbital.

Introduction

Transition-metal complexes exhibiting "spin crossover" between thermally populated low- and high-spin states have been recognized since Cambi et al. first observed "magnetic isomerism" for the tris(dithiocarbamato)iron(III) complexes in 1931.[1] Since then, a number of spin-crossover complexes of Fe(III),[2-4] Fe(II),[5,6] and Co(III),[7] etc., have been studied.

(1) L. Cambi, L. Szego, and A. Cagnasso, *Atti Accad. Naz. Lincei, Cl. Sci. Fis., Mat. Nat. Rend.*, **15**, 266 (1932).

0020-1669/84/1323-2440$01.50/0

The initial studies focused upon the anomalous magnetic behavior in the solid state. As the magnetism is a gross property of the complex, the electronic behavior of each molecule cannot be studied directly. However, Mössbauer absorption spectroscopy has proved to be an extremely powerful tool for studying the electronic state in the Mössbauer lifetime.

In the case of the spin-crossover phenomenon observed in the solid state, the complexes can be mainly classified into two groups according to their transition behavior: (i) the complexes of the first group show dynamic spin equilibrium, the interchange of the spin state. (ii) The complexes of the second group show transition of the spin state depending on temperature. The transition of this type may be connected with a first-order transition, a cooperative phase transition in the solid state.[8,9]

Tris(*N*,*N*-dialkyldithiocarbamato)iron(III) shows the interchange between the ^6A and ^2T states. A series of these complexes were first prepared by Delepine,[10] and their anomalous magnetic behavior was confirmed by Cambi et al.[1] The Mössbauer spectra for these compounds were measured at various temperatures by Rickards et al.[11] and the other workers.[12,13] However, only one poorly split doublet was observed above 78 K. These phenomena have been interpreted by the model that the electronic relaxation time between the high- and low-spin states is faster than the ^{57}Fe Mössbauer lifetime (1×10^{-7} s), thus the iron nucleus "sees" an average of the properties of both states, and that the values of the Mössbauer parameters are averaged and depend on the population of each form. Many explanations have been given for these spin-transition mechanisms.[14-16] A spin-equilibrium phenomenon populated thermally between the high- and low-spin states was also confirmed by the application of X-ray photoelectron[17] and IR spectroscopies.[18]

The spin-crossover phenomenon in solution has also been established by using either the Evans NMR method,[19] the laser Raman temperature-jump method, or the ultrasonic experiments[20,21] and has been modeled in terms of an internal electron-transfer reaction with a lifetime of $30 \lesssim \tau \lesssim 120$ ns.

Experimental Section

The magnetic susceptibility data on the polycrystalline samples at various temperatures (80–300 K) were obtained by the Faraday method, using an instrument described elsewhere.[3] The magnetic susceptibilities were calibrated by the use of $HgCo(NCS)_4$, corrected for the diamagnetism of the ligands and anions, and the effective magnetic moments were calculated by the formula $\mu_{eff} = 2.84(\chi_M T)^{1/2}$, χ_M being a corrected molar magnetic susceptibility and T a temperature in K.

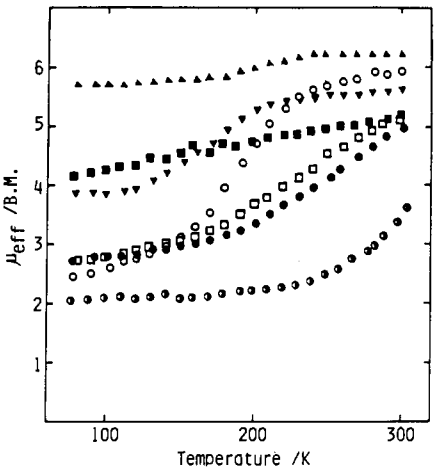

Figure 1. Effective magnetic moment vs. temperature plots for the iron(III) complexes: (▲) $[Fe(vapa)_2]PF_6$; (▼) $[Fe(sapa)_2]NO_6 \cdot {}^3/_2H_2O$; (○) $[Fe(acpa)_2]PF_6 \cdot H_2O$; (●) $[Fe(acpa)_2]BPh_4 \cdot H_2O$; (◑) $[Fe(acpa)_2]NO_3 \cdot H_2O$; (□) $[Fe(bzpa)_2]PF_6 \cdot 2H_2O$; (■) $[Fe(bzpa)_2]BPh_4 \cdot 2H_2O$.

The EPR powder measurements were performed with a FES-FEX (JEOL, Ltd.) spectrometer at the X-band frequencies. The magnetic field was calibrated with a 2,2-diphenyl-1-picrylhydrazyl or Mn marker.

Mössbauer spectroscopy was effected by using an instrument described elsewhere.[3] All isomer shifts are reported with respect to the centroid of the spectrum of an iron foil enriched with ^{57}Fe at 295 K, which was also used as a standard material for velocity calibration. All spectra were fitted to the Lorentzian line shapes by using the least-square method at the Computer Center, Kyushu University.

The electronic spectra of the acetone solution containing the samples (3×10^{-3} mol/L) were recorded on a Hitachi photospectrometer, Model EPS-3T. The solution conductivities were measured in nitromethane containing the sample (1×10^{-3} mol/L) at 25 °C by using a Yanagimoto Conductivity Outfit, Model MY-8. The comparative value for a nitromethane solution of $(Et_4N)ClO_4$ (1×10^{-3} mol/L) is 80 μmho/cm.

Compound Preparation. All elemental analyses of the complexes were performed in the Elemental Analysis Center, Kyushu University.

$[Fe(sapa)_2]NO_3 \cdot {}^3/_2H_2O$. This complex was prepared according to the literature;[22] $\Lambda = 82$ μmho/cm. Anal. Calcd for $FeC_{26}H_{25}N_5O_{6.5}$: C, 55.04; N, 12.34; H, 4.41. Found: C, 54.75; N, 12.13; H, 4.07.

$[Fe(acpa)_2]PF_6 \cdot H_2O$. The Hacpa ligand was prepared by adding 2-(aminomethyl)pyridine (2.16 g, 20 mmol) in 20 mL of methanol to a solution of acetylacetone (2.00 g, 20 mmol) in 20 mL of methanol. Then, the solution was refluxed until it turned yellow. $NaOCH_3$ (1.08 g, 20 mmol) dissolved in 50 mL of methanol was added to this solution, and the solution was stirred for an additional 15 min. To this solution was slowly added $Fe(NO_3)_3 \cdot 9H_2O$ (4.04 g, 10 mmol) dissolved in 15 mL of methanol, producing a color change from yellow to blue-violet. After 10 min, the solution was filtered and NH_4PF_6 (3.2 g, 20 mmol) in 20 mL of methanol was added. After the solution was evaporated under reduced pressure and then cooled, the product of the blue-black solid was collected by filtration and washed with methanol. The crude products were recrystallized from acetone/methanol solution (1:1 by volume), and the resulting blue-violet crystals were washed with methanol and ether and dried in vacuo over P_2O_5; $\Lambda = 103$ μmho/cm. Anal. Calcd for $FeC_{22}H_{28}N_4O_3PF_6$: C, 44.24; N, 9.38; H, 4.69. Found: C, 44.59; N, 9.12; H, 4.70.

$[Fe(acpa)_2]BPh_4 \cdot H_2O$. This complex was prepared by the metathesis of the nitrate salt with $NaBPh_4$ in methanol; $\Lambda = 67$ μmho/cm. Anal. Calcd for $FeC_{46}H_{48}N_4O_3B$: C, 71.63; N, 7.26; H, 6.23. Found: C, 71.73; N, 7.09; H, 6.15.

The other iron complexes were prepared by a similar method. The analytical and conductivity data are as follows. For $[Fe(vapa)_2]PF_6$, $\Lambda = 100$ μmho/cm. Anal. Calcd for $FeC_{28}H_{26}N_4O_4PF_6$: C, 49.20;

(2) P. Gütlich, *Struct. Bonding (Berlin)*, **44**, 83 (1981).
(3) H. Ohshio, Y. Maeda, and Y. Takashima, *Inorg. Chem.*, **22**, 2684 (1983).
(4) A. H. Ewald, R. L. Martin, I. G. Ross, and A. H. White, *Proc. R. Soc. London, Ser. A*, **280**, 235 (1964).
(5) I. Dézsi, B. Molnár, T. Tarnóczi, and K. Tompa, *J. Inorg. Nucl. Chem.*, **29**, 2486 (1967).
(6) E. König, G. Ritter, W. Irler, and H. A. Goodwin, *J. Am. Chem. Soc.*, **102**, 4681 (1980).
(7) S. Kremer, W. Henke, and D. Reinen, *Inorg. Chem.*, **21**, 3013 (1982).
(8) M. Sorai and S. Seki, *J. Phys. Chem. Solids*, **35**, 555 (1974).
(9) P. Gütlich, H. Koppen, R. Link, and H. G. Steinhauser, *J. Chem. Phys.*, **70**, 3977 (1979).
(10) M. Delepine, *Bull. Soc. Chim. Fr.* **3** (4), 643 (1908).
(11) R. Rickards, C. E. Johnson, and H. A. O. Hill, *J. Chem. Phys.*, **48**, 5231 (1968).
(12) L. M. Epstein and D. K. Straub, *Inorg. Chem.*, **8**, 784 (1969).
(13) R. M. Golding and H. J. Whitfield, *Trans. Faraday Soc.*, **62**, 1713 (1966).
(14) P. B. Merrithew and P. G. Rasmussen, *Inorg. Chem.*, **11**, 325 (1972).
(15) G. Harris, *Theor. Chim. Acta*, **10**, 119 (1968).
(16) N. Sasaki and T. Kambara, *J. Chem. Phys.*, **74**, 3472 (1981).
(17) M. J. Tricker, *J. Inorg. Nucl. Chem.*, **36**, 1543 (1974).
(18) R. J. Butcher, J. R. Ferraro, and E. Sinn, *Inorg. Chem.*, **15**, 2077 (1976).
(19) M. A. Hoselton, L. J. Wilson, and R. S. Drago, *J. Am. Soc.*, **97**, 1722 (1975).
(20) K. A. Reeder, E. V. Dose, and L. J. Wilson, *Inorg. Chem.*, **17**, 1071 (1978).
(21) J. K. Beattie, R. A. Binstead, and R. J. West, *J. Am. Chem. Soc.*, **100**, 3044 (1978).
(22) R. W. Oehmke and J. C. Bailar, Jr., *J. Inorg. Nucl. Chem.*, **27**, 2209 (1965).

Table I. Thermodynamics and Crossover Parameters for Iron(III) Complexes

complex	ΔH°,[a] kcal/mol	ΔS°,[b] eu	log C' [c]
$[Fe(sapa)_2]NO_3 \cdot {}^3/_2H_2O$	1.43	9	1.55
$[Fe(acpa)_2]NO_3 \cdot H_2O$	3.56	9	1.58
$[Fe(acpa)_2]PF_6 \cdot H_2O$	3.48	18	3.59
$[Fe(acpa)_2]BPh_4 \cdot H_2O$	2.43	10	1.74
$[Fe(bzpa)_2]PF_6 \cdot 2H_2O$	2.64	10	1.75

[a] Enthalpy change for the spin transition. [b] Entropy change for the spin transition. [c] Ratio of the molecular partition functions in the two states.

N, 8.20; H, 3.81. Found: C, 49.03; N, 8.35; H, 3.92. For $[Fe(acpa)_2]NO_3 \cdot H_2O$, Λ = 97 μmho/cm. Anal. Calcd for $FeC_{22}H_{28}N_5O_6$: C, 51.37; N, 13.62; H, 5.45. Found: C, 51.75; N, 13.81; H, 5.27. For $[Fe(bzpa)_2]PF_6 \cdot 2H_2O$, Λ = 94 μmho/cm. Anal. Calcd for $FeC_{32}H_{34}N_4O_4PF_6$: C, 51.97; N, 7.58; H, 4.33. Found: C, 52.33; N, 7.41; H, 4.25. For $[Fe(bzpa)_2]BPh_4 \cdot 2H_2O$, Λ = 64 μmho/cm. Anal. Calcd for $FeC_{56}H_{54}N_4O_4B$: C, 73.63; N, 6.13; H, 5.92. Found: C, 73.12; N, 6.05; H, 5.57.

Results and Discussion

(a) Characterization of the Complexes. The complexes used here are confirmed as pseudooctahedral iron(III) complexes with the FeN_4O_2 coordination core from elemental analysis and characterized as salts, which are uni-univalent electrolytes as given in the Experimental Section.

(b) Magnetic Susceptibility. The values of magnetic moments for the complexes at room temperture span a range of from ca. 2 to ca. 6 μ_B. This anomalous magnetic behavior can be interpreted by examining the temperature-dependent magnetic susceptibility shown in Figure 1. The magnetic moment of $[Fe(vapa)_2]PF_6$ is characteristic of high-spin Fe(III) complexes. The other compounds exhibit the property of a spin-crossover transition.

The high-spin population (x) at a certain temperature is obtained by assuming a simple additive property in magnetic susceptibilities, and the equilibrium constant can be obtained by $K = x/(1 - x)$. The changes of the enthalpy (ΔH) and entropy (ΔS) accompanying the spin transition are evaluated by using the equation $\ln K = -\Delta H/RT + \Delta S/R$.

The effective magnetic moment, μ_{eff} is calculated by[23]

$$\mu_{eff}^2 = \{0.75g^2 + 8x^{-1}[1 - \exp(-3x/2)] + 105C' \exp[-(1 + E/\zeta)x]\}/\{1 + 2\exp(-3x/2) + 3C' \exp[-(1 + E/\zeta)x]\}$$

where E is the separation energy between zero-point levels of the low- and high-spin states, ζ is the one-electron spin–orbit coupling constant, $x = \zeta/kT$, and C' is the ratio of the molecular vibrational partition functions in the ^6A and ^2T states. The value of log C' is evaluated from the equilibrium constant and the experimental g value obtained from EPR data. The best fit parameters for the complexes calculated by the least-squares method and kinetic data are summarized in Table I. The values of ΔH and ΔS calculated for these complexes are identical with those found for other spin-crossover complexes in solution, and likewise there are no remarkable differences from those for other spin-crossover complexes that do not show the spin-equilibrium phenomenon on the Mössbauer spectra. The ΔH value mainly reflects the changes of iron(III)-donor atom bond distances. It is doubtful, however, whether the differences in these values can be attributed to the differences of the mechanism of the spin-state transition.

(c) Mössbauer Spectra. Mössbauer spectra for these compounds were measured to characterize the electronic states and properties of the spin-crossover phenomena. Figure 2 shows the spectra for $[Fe(sapa)_2]NO_3 \cdot {}^3/_2H_2O$ at 290 and 80 K, in

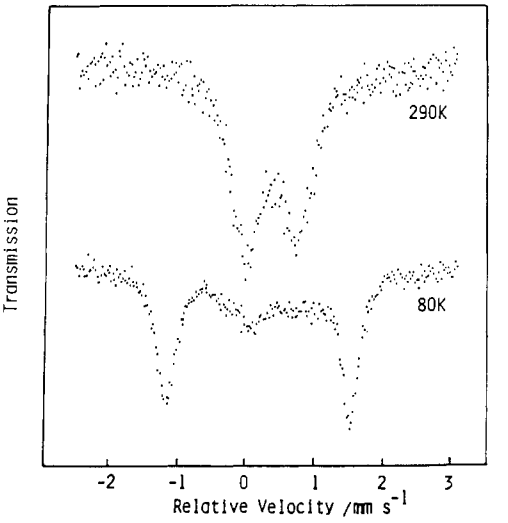

Figure 2. Mössbauer spectra for $[Fe(sapa)_2]NO_3 \cdot {}^3/_2H_2O$ at 80 and 290 K.

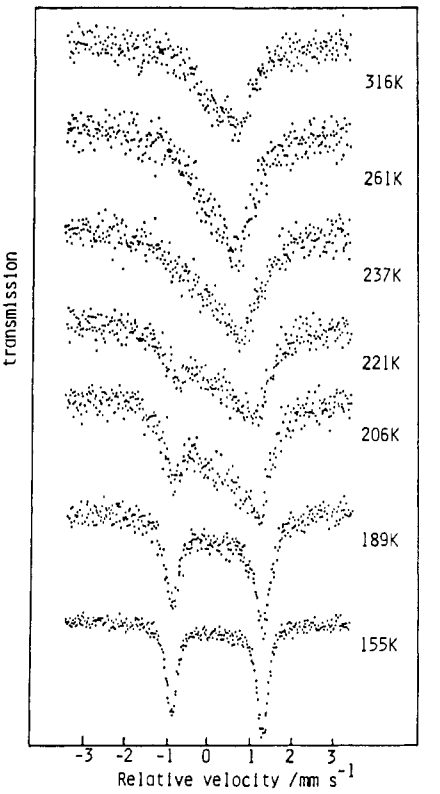

Figure 3. Mössbauer spectra for $[Fe(acpa)_2]PF_6 \cdot H_2O$ at various temperatures.

which the spectrum at 290 K consists of a well-resolved doublet due to the high-spin iron(III) ($S = {}^5/_2$, the isomer shift IS = 0.344 mm/s, quadrupole splitting QS = 0.620 mm/s), while the spectrum at 80 K shows the superposition of the two doublets in accordance with the magnetic data; a new outer doublet (IS = 0.188 mm/s, QS = 2.701 mm/s) is characteristic of low-spin iron(III) ($S = {}^1/_2$). Similar fast-spin-transition behavior is observed for $[Fe(bzpa)_2]BPh_4 \cdot 2H_2O$. The Mössbauer data for the complexes that do not show the fast spin interconversion are listed in Table II.

The Mössbauer spectra for $[Fe(acpa)_2]PF_6 \cdot H_2O$ at various temperatures are shown in Figure 3, and the Mössbauer parameters evaluated are listed in Table III. The spectra between 80 and 155 K are characterized by the values QS = 2.24–2.19 mm/s and IS = 0.25–0.23 mm/s. However, a new doublet becomes visible at 189 K and gains in intensity with

(23) A. H. Ewald, R. L. Martin, E. Sinn, and A. H. White, *Inorg. Chem.*, 8, 1837 (1969).

Table II. Mössbauer Parameters for Several Complexes

complex	T, K	IS,[a] mm/s	QS,[b] mm/s	Γ,[c] mm/s		S,[d] %
$[Fe(sapa)_2]NO_3 \cdot {}^3/_2H_2O$	290	0.344	0.620	0.690	0.854	
	80	0.410	0.946	0.857	0.840	43.4
		0.188	2.701	0.351	0.299	56.6
$[Fe(vapa)_2]PF_6$	295	0.340	0.784	0.630	1.393	
	80	0.456	0.762	0.520	1.015	
$[Fe(acpa)_2]NO_3 \cdot H_2O$[e]	317	0.214	1.305	0.774	0.450	
	287	0.171	1.839	0.488	0.391	
	80	0.216	2.253	0.260	0.257	
$[Fe(bzpa)_2]BPh_4 \cdot 2H_2O$	295	0.264	0.612	0.621	0.621	
	80	0.325	0.434	0.843	0.843	52.4
		0.193	2.080	0.754	0.754	47.6

[a] Isomer shift. [b] Quadrupole splitting. [c] Full width at half-maximum. [d] Relative peak area under the resonance curve. [e] This complex shows the behavior of fast spin interconversion.

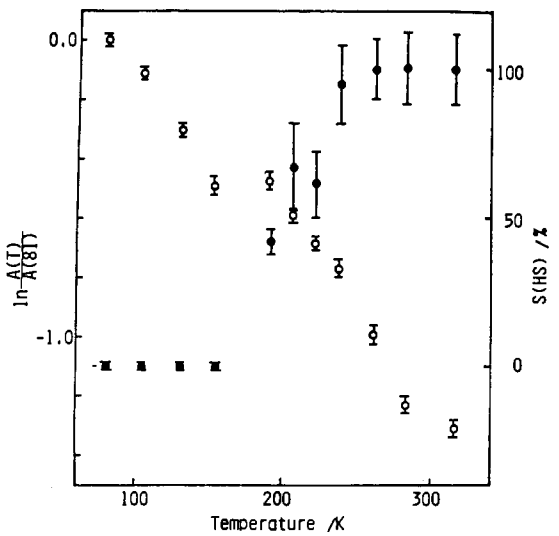

Figure 4. Temperature dependence of the ln $(A(T)/A(81))$ (○) and $S(HS)$ (●) parameters for $[Fe(acpa)_2]PF_6 \cdot H_2O$.

the rising of temperature, while the initial doublet simultaneously decreases its intensity. A line width becomes broad above 237 K, and the IS value above 237 K is characteristic of a high-spin state. Figure 4 illustrates the temperature dependence of the area fraction of a high-spin species $S(hs)$ vs. the total absorption area. This curve is consistent with that of the temperature dependence of the population probability of the high-spin species calculated from the magnetic data, on the assumption that $\mu_{eff}(hs) = 5.9\ \mu_B$ and $\mu_{eff}(ls) = 2.0\ \mu_B$. The temperature dependence of a recoil-free fraction is given by the temperature dependence of the area under the resonance curve. The Debye model approximation in the high-temperature limit leads to the hypothesis[24]

$$d \ln f/dT \propto d \ln A/dT$$

where A is a normalized absorption area. The plot of ln $(A(T)/A(81))$ vs. T for $[Fe(acpa)_2]PF_6 \cdot H_2O$ is shown in Figure 4, and discontinuity in the curve is observed in the temperature range between 155 and 189 K. It can be presumed that some changes in the lattice (i.e., some kinds of phase) transition occur in this temperature range, if spin transition accompanies the intermolecular or lattice vibrational change. The fact that two pairs of a doublet are observed in the Mössbauer spectra means that the spin interconversion between the low- and high-spin states, the electronic relaxation of the spin transition, is slow relative to the lifetime of the excited Mössbauer nuclear state (1×10^{-7} s). The full width

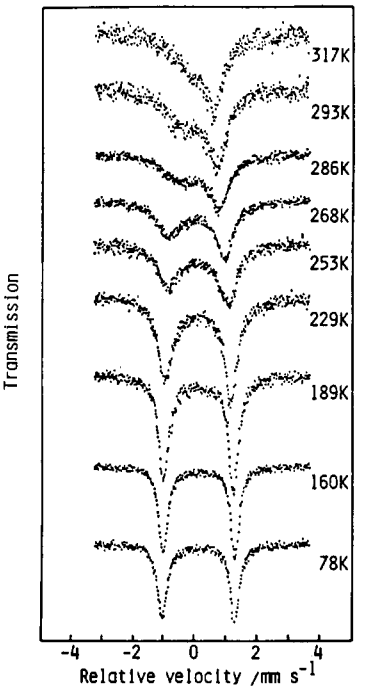

Figure 5. Mössbauer spectra for $[Fe(acpa)_2]BPh_4 \cdot H_2O$ at various temperatures.

at half-maximum (fwhm) of the high-spin isomers becomes large at high temperature, and the spectra between 316 and 261 K do not show the well-resolved component. This phenomenon is also observed in the Mössbauer spectra for $[Fe(acpa)_2]BPh_4 \cdot H_2O$ and $[Fe(bzpa)_2]PF_6 \cdot 2H_2O$.

The Mössbauer spectra for $[Fe(acpa)_2]BPh_4 \cdot H_2O$ at various temperatures are shown in Figure 5. The spectra between 78 and 189 K are typical for the low-spin iron(III) complexes, and an absence of the excessive spectral broadening at low temperature indicates that the antiferromagnetism does not contribute to the anomalous magnetic behavior. The spectrum at 317 K is characterized by a broad asymmetric doublet with IS = 0.402 mm/s ascribed to a high-spin iron(III) state. Only one doublet with broad line widths is observed above 200 K. The temperature dependence of the IS value below 200 K (-2.99×10^{-4} mm/(s K)) is lower than that expected from the second-order Doppler effect (-7.3×10^{-4} mm/(s K)). The rising of the IS value above 286 K suggests a change of spin state from a low-spin to a high-spin ground state. A peak width asymmetry ($\Gamma_h/\Gamma_l = 0.29$ at 317 K on the basis of one doublet analysis) is observed at high temperature, but the extent of the peak area asymmetry ($I_h/I_l = 0.95$ at 317 K) is not appreciable. The temperature dependence of the peak width asymmetry has to be explained in terms of a relaxation mechanism (the effect of fluctuating magnetic hyperfine fields) in which the relaxation time increases with increasing temperature.[25] This mechanism causes substantial broadening of one line in comparison with the other. Since the nuclear precession times for the $\pm{}^1/_2 \rightarrow \pm{}^3/_2$ transitions are shorter than for the $\pm{}^1/_2 \rightarrow \pm{}^1/_2$ transitions when the hyperfine field axis is parallel to the principal axis of the electric field gradient (V_{zz}), one can expect that the relaxation broadening will be greater for the $\pm{}^1/_2 \rightarrow \pm{}^3/_2$ transition line. However, the sign of the principal axis of electric field gradient is not firmly fixed for this complex because the orientation relation (parallel or perpendicular) between the hyperfine field axis and V_{zz} is not settled.

It is concluded from the Mössbauer spectra for $[Fe(acpa)_2]BPh_4 \cdot H_2O$ that the electron transfer from one state

(24) R. H. Herber and Y. Maeda, *Physica B + C (Amsterdam)* **99B**, 352 (1980).

(25) S. V. Karyagin, *Dokl. Akad. Nauk SSSR*, **148**, 1102 (1963).

Table III. Mössbauer Parameters for $[Fe(acpa)_2]PF_6 \cdot H_2O$ at Various Temperatures

	low-spin isomer				high-spin isomer				
T, K	IS, mm/s	QS, mm/s	Γ, mm/s	S, %	IS, mm/s	QS, mm/s	Γ, mm/s	S, %	ln $(A(T)/A(81))$
81	0.248	2.236	0.315 0.306	46.7 53.3 } 100.0					0.0
104	0.246	2.232	0.324 0.314	45.8 51.4 } 100.0					−0.115
130	0.245	2.206	0.300 0.289	46.2 53.8 } 100.0					−0.313
155	0.233	2.190	0.317 0.329	44.5 55.5 } 100.0					−0.492
189	0.208	2.167	0.389 0.389	28.9 28.9 } 57.8	0.571	0.895	1.283 0.798	25.4 16.9 } 42.2	−0.479
206	0.202	2.105	0.549 0.422	18.8 14.3 } 33.1	0.446	0.815	1.102 1.069	42.6 24.3 } 66.9	−0.589
221	0.203	1.983	0.627 0.627	19.2 19.2 } 38.4	0.361	0.762	1.058 0.793	43.9 17.7 } 61.6	−0.658
237	0.202	2.100	0.236 0.236	2.3 2.3 } 4.6	0.378	0.805	1.539 0.802	52.6 42.8 } 95.4	−0.756
261					0.291	0.740	1.077 0.919	65.6 34.4 } 100.0	−1.000
283					0.330	0.663	0.894 0.801	58.2 41.8 } 100.0	−1.232
316					0.333	0.636	1.046 0.614	58.4 41.6 } 100.0	−1.315

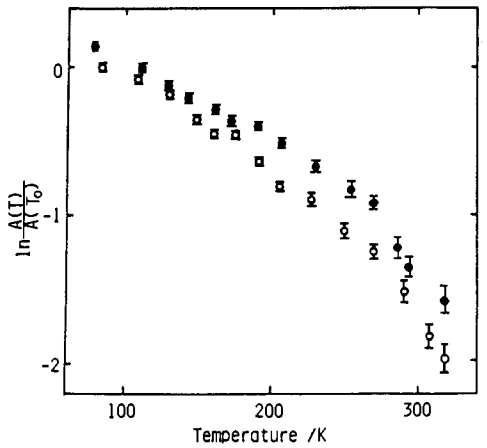

Figure 6. Temperature dependence of the ln $(A(T)/A(T_0))$ parameters for $[Fe(bzpa)_2]PF_6 \cdot 2H_2O$ (○) and $[Fe(acpa)_2]BPh_4 \cdot H_2O$ (●).

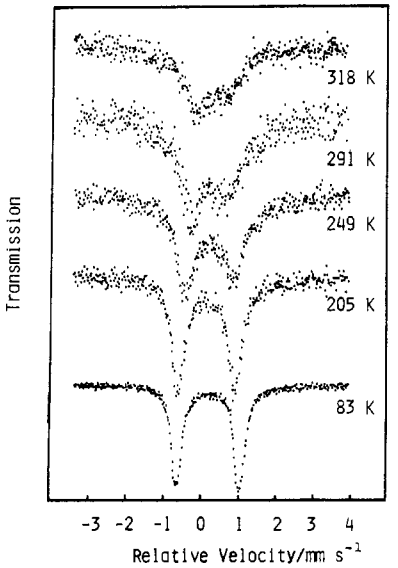

Figure 7. Mössbauer spectra for $[Fe(bzpa)_2]PF_6 \cdot 2H_2O$ at various temperatures.

to the other can proceed as fast as 10^7 s^{-1} or more although the electron transfer is accompanied by a change in the spin multiplicity (spin-forbidden transition). Examples of fast spin interconversion have been observed for many complexes in

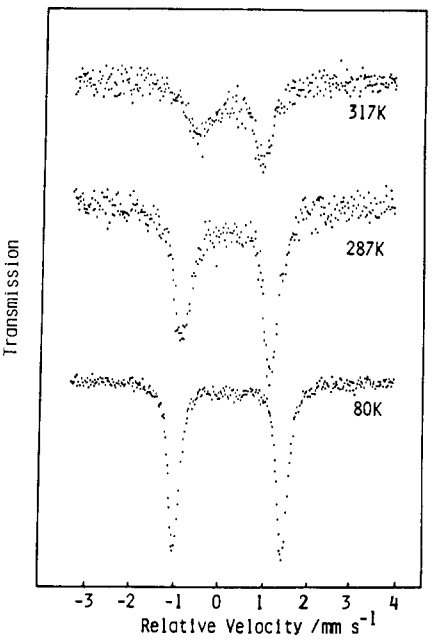

Figure 8. Mössbauer spectra for $[Fe(acpa)_2]NO_3 \cdot H_2O$ at various temperatures.

solution. However, it was pointed out by Merrithew and Rasmussen that the fast transition velocity of 10^7 s^{-1} is not characteristic of the complexes with different spin states.[14] In contrast, Harris[15] provides support for the existence of a mixed-spin state of varying characters. The rate-determining step for spin conversion is assumed not to be electric in origin but to involve the rearrangement of the coordination sphere. The rearrangement of the coordination sphere for the complex would demand a very small change in geometry because no gap is observed in the temperature dependence of ln $(A(T)/A(110))$ as shown in Figure 6.

The rapid spin-state transition is also observed in the Mössbauer spectra of $[Fe(bzpa)_2]PF_6 \cdot 2H_2O$ (Figure 7). The spectra in the temperature region of the spin-state transition are characterized by only one doublet. The peak width asymmetry for this complex at 318 K is opposite of that for $[Fe(acpa)_2]BPh_4 \cdot H_2O$; the broad component appears in the positive velocity region. This fact may suggest that the geometry of FeN_4O_2 in $[Fe(bzpa)_2]^+$ is different from that in the $[Fe(acpa)_2]^+$.

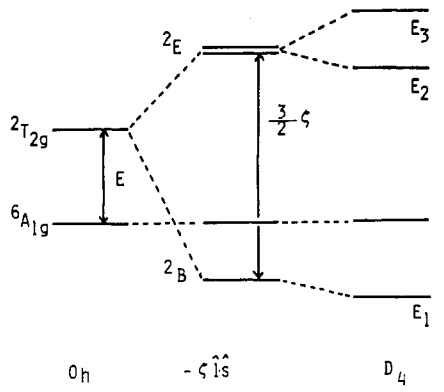

Figure 9. Energy level diagram for the spin-crossover iron(III) system: O_h, crystal field (O_h symmetry) interaction; $-\zeta\hat{l}\cdot\hat{s}$, spin–orbit coupling interaction; D_4, rhombic distortion (from O_h symmetry) interaction.

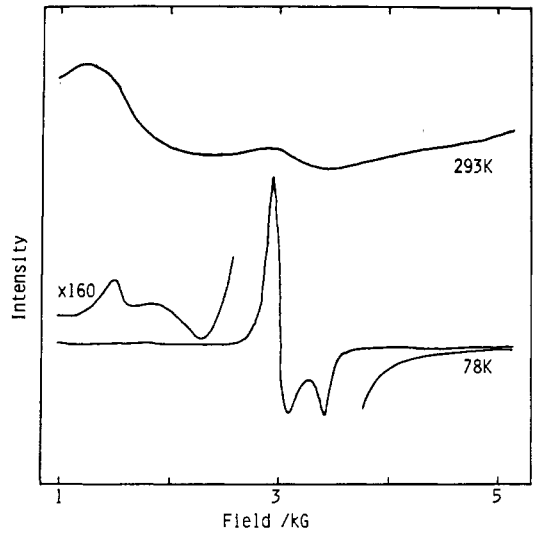

Figure 10. EPR spectra for $[Fe(acpa)_2]BPh_4 \cdot H_2O$ at 78 and 293 K.

Figure 8 shows the Mössbauer spectra of $[Fe(acpa)_2]NO_3 \cdot H_2O$ at various temperatures. The spectral shape at 317 K is similar to that for $[Fe(acpa)_2] \cdot BPh_4 \cdot H_2O$, and the fast spin-state transition is observed above ca. 290 K. It is concluded that two iron complexes with the ligand acpa shows the fast spin-state transition and the rates of the spin interchange vary with the species of the anion of the complex. The rates of the spin interconversion and the spin-transition temperature (defined as the temperature at which there are equal populations of the low-spin and high-spin states) depend significantly on anions; however, no systematic conclusion was found.

(d) Electron Paramagnetic Resonance. The EPR signals were difficult to observe for the spin-crossover complex tris(dithiocarbamato)iron(III) and could only be effectively recorded at the liquid-helium temperature.[26] Haddad et al.[27] discussed the electronic state of a spin-crossover complex $[Fe(X\text{-}SalEen)_2]Y$. The energy level diagram for octahedral spin-crossover iron(III) complexes is shown in Figure 9. The separation energy E was considered as a temperature-independent parameter in this paper.

The temperature profiles of the EPR spectra for the iron complexes with acpa were found to be similar to each other except for the relative intensities of signals. The two signals, one at g = ca. 4 and the other g = ca. 2 are observed at room temperature (Figure 10). The g = ca. 4 signal for high-spin iron(III) is observed for the complexes with the low symmetry (rhombic) because the zero-field splitting in the high-spin state is gauged by $H = DS_z^2 + E(S_x^2 - S_y^2)$, where D and E are the axial and rhombic zero-field splitting parameters, respectively. A complex with rhombic symmetry exhibits an intense $g = 4.3$ signal if $E/D \simeq {}^1/_3$ and $h\nu/D \leq 3$.[28] At low temperature, the g = ca. 2 signal is well resolved, increases in intensity relative to the other signal, and is characterized by axial symmetry in contrast with rhombic symmetry in a high-spin state. The difference of the molecular symmetry between the low- and high-spin states would play an important role in the spin-exchange mechanism. Table IV gives the g values of the low-spin state of these complexes.

Table IV. Experimental and Calculated EPR Parameters[a]

	$[Fe(acpa)_2]BPh_4 \cdot H_2O$	$[Fe(acpa)_2]PF_6 \cdot H_2O$
g_x	2.245	2.220
g_y	2.245	2.220
g_z	1.928	1.954
δ/ζ	2.31	2.83
ϵ/ζ	0	0
A_1	0.108	0.094
B_1	0.993	0.996
C_1	0	0
E_1/ζ	−4.696	−5.602
A_2	0.994	0.996
B_2	0.109	0.089
C_2	0	0
E_2/ζ	1.886	2.268
A_3	0.996	0.997
B_3	0.095	0.078
C_3	0	0
E_3/ζ	2.810	3.334

[a] A_1, B_1, C_1, and E_1, for ground state; A_2, B_2, C_2, and E_2, for first excited state; A_3, B_3, C_3, and E_3, for second excited state.

The signals similar to that for $[Fe(acpa)_2]^+$ species were observed for $[Fe(bzpa)_2]^+$ species at room temperature. However, the signals become weak in intensity at low temperatures, and the g = ca. 2 signal for the low-spin state was almost unresolved or disappeared at 120 K in contrast with the EPR spectra for $[Fe(acpa)_2]^+$.

It is possible to use the g values to elucidate the nature of the ground state of ^2T for the $[Fe(acpa)_2]^+$ species. The spin–orbit coupling and crystal field distortion interactions shown in Figure 9 were considered in this calculation. The six spin–orbit distortion matrix eigenfunctions may be given as[29]

$$\Psi_i = A_i|+1^+\rangle + B_i|\zeta^-\rangle + C_i|-1^+\rangle$$
$$\Psi_i = A_i|-1^-\rangle - B_i|\zeta^+\rangle + C_i|+1^-\rangle \quad (1)$$

where i = 1–3 and $\zeta = 1/(2^{1/2})(|2\rangle - |-2\rangle)$. In the above expressions, the parameters A_i, B_i, and C_i are the functions of ζ, δ, and ϵ, where ζ is the one-electron spin–orbit coupling constant, δ is the distortion parameter due to an axial distortion, and ϵ is due to any lower distortion. The Kramers doublet will be split by the magnetic field interaction, and this interaction will be given by a Zeeman Hamiltonian $\mathcal{H} = \beta(kl + 2s)H$, where k is the orbital reduction factor. By considering the matrix elements of a Zeeman Hamiltonian, the secular equations can be solved to give the wave functions[29]

$$g_z = 2[A^2 - B^2 + C^2 + k(A^2 - C^2)]$$
$$g_x = -2[2AC - B^2 + kB(2^{1/2})(C - A)]$$
$$g_y = 2[2AC + B^2 + kB(2^{1/2})(C + A)]$$

(26) G. R. Hall and D. N. Hendrickson, *Inorg. Chem.*, **15**, 607 (1976).
(27) M. S. Haddad, M. W. Lynch, W. D. Federer, and D. N. Hendrickson, *Inorg. Chem.*, **20**, 123 (1981).
(28) H. H. Wickman, M. P. Klein, and D. A. Shirley, *J. Chem. Phys.*, **42**, 2113 (1965).
(29) R. M. Golding, "Applied Wave Mechanics", Van Nostrand Ltd., London, 1969.

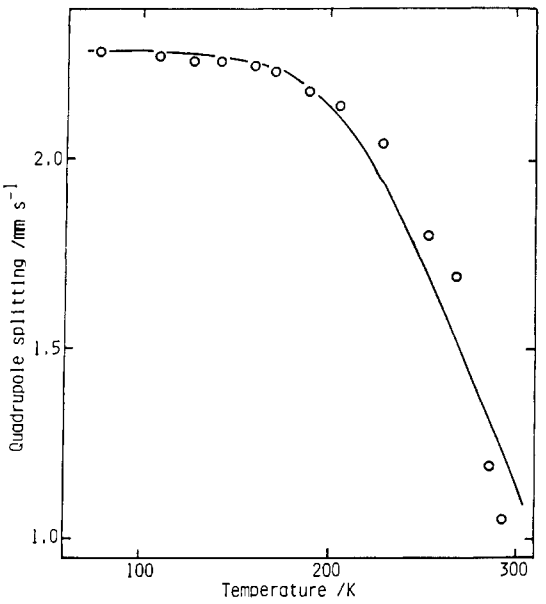

Figure 11. Temperature dependence of the observed quadrupole splitting and theoretical line calculated with the parameters listed in the text for $[Fe(acpa)_2]BPh_4 \cdot H_2O$.

Assuming the value of 0.9 for k, the values of A, B, and C were determined by using the observed g values. The reasonable values were selected and listed in Table IV. The fact that the B_1 value is largest in the ground state indicates that the ground-state Kramers doublet consists mainly of the state wherein the unpaired electron resides in the d_{xy} orbital. This is in agreement with the origin of the large quadrupole splitting for the $[Fe(acpa)_2]^+$ species. If the appropriate one-electron orbitals for the ^2T configuration are employed with the Hamiltonian[29]

$$\mathcal{H} = -\zeta\hat{l}\cdot\hat{s} - (\hat{l}_z^2 - 2) - (\epsilon/2)(\hat{l}_+^2 + \hat{l}_-^2)$$

then a set of three secular equations brings about the ground-state Kramers doublet. The ratios δ/ζ and ϵ/ζ may be determined by using the values of A_i, B_i, and C_i, as summarised in Table IV.

From the parameters A_i, B_i, C_i, E_i/ζ, and C' obtained from the magnetic data, the temperature dependence of the quadrupole splitting (TQS) was evaluated for $[Fe(acpa)_2]BPh_4 \cdot H_2O$ by using the relation[3]

$$E_Q = \frac{\sum_i \Delta E_{Q_i} \exp(-E_i/kT)}{\sum_i \exp(-E_i/kT) + 3C' \exp(-E/kT)}$$

ΔE(lat) = 0.21 mm/s, E = 281 cm^{-1}, and ζ = 176 cm^{-1} were evaluated by fitting the equation to experimental measurements. The lattice contribution ΔE(lat) was assumed to be equal between the ^2T and ^6A states in this calculation. Figure 11 shows the plots of the experimental data and curve calculated with the best fit values listed in Table IV. The ligand field and crossover parameters calculated for this fast spin-interconversion system are similar to those for the slow spin-conversion system.

(e) Spin-Interconversion Rate. The simulation of the Mössbauer spectra was carried out in order to measure directly the spin-interconversion rate constants and spin-state lifetimes in the solid state. The mathematical formalism that was applied to this relaxation model is based on the quantum-mechanical density matrix equations of motion dG_i/dt given by Wickman.[30] The theoretical Mössbauer spectra is calculated from the equation of motion expressed by eq 2, in which the subcripts i refer to an individual Mössbauer transition

$$I(\omega) = \sum_i K'[(1 + \tau\Gamma)P_i + Q_iR_i/(P_i^2 + R_i^2)] \quad (2)$$

where

$$P_i = \tau\{\Gamma^2 - [\tfrac{1}{2}(\omega_i^h + \omega_i^l) - \omega]^2 + \tfrac{1}{4}(\omega_i^h - \omega_i^l)^2\} + \Gamma$$

$$Q_i = \tau[\tfrac{1}{2}(\omega_i^h + \omega_i^l) - \omega - \tfrac{1}{2}(p_h - p_l)(\omega_i^h - \omega_i^l)]$$

$$R_i = [\tfrac{1}{2}(\omega_i^h + \omega_i^l) - \omega](1 + 2\tau\Gamma) + \tfrac{1}{2}(p_h - p_l(\omega_i^h - \omega_i^l)]$$

The constance K' is the relative intensity of the ith transition, and p_h and p_l are the populations of the high- and low-spin isomers, respectively. In our model, the relaxation process occurs between the high- and low-spin energy levels. The line width was set at 0.35 mm/s for all calculations. In fitting the experimental spectra to this model the isomer shifts, line intensities, and populations of the high-spin species were parameterized as well as the relaxation time. The computer minimizations of eq 2 result in the theoretical spectra presented in Figure 12. The fit is good at low temperatures (<268 K) because the increase of the population of the ^6A state makes the line width broad due to the spin–spin relaxation and spin–lattice relaxation. Therefore, the calculated relaxation times may be convincing only at low temperatures. The lifetime of the low-spin state is shown by τ_l. The observed relaxation times ($\tau = \tau_l\tau_h/(\tau_l + \tau_h)$) span a range from 6.9 × 10^{-7} to 1.6 × 10^{-5} s and are dependent on temperature (268–189 K). The rates forward k_1 and reverse k_{-1} for the spin-conversion intersystem crossing for the dynamic

$$^2T \underset{k_{-1}}{\overset{k_1}{\rightleftharpoons}} {}^6A$$

are defined as $1/\tau_l$ and $1/\tau_h$, respectively, and the equilibrium constant $K'' = k_1/k_{-1}$. The activation energy of the spin-conversion crossing 2.4 kcal/mol is evaluated by a plot of the log K'' vs. $1/T$ for $[Fe(acpa)_2]BPh_4 \cdot H_2O$.

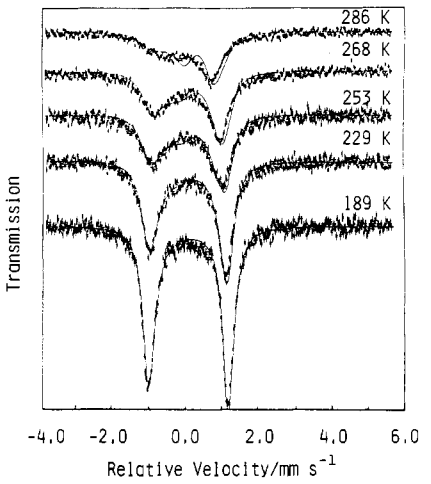

Figure 12. Representative attempt to obtain a best fit between the Mössbauer spectra for $[Fe(acpa)_2]BPh_4 \cdot H_2O$ and the model. The full curves are calculated by using the following parameters: 286 K, p_h = 0.60, τ_l = 3.4 × 10^{-7} s; 268 K, p_h = 0.42, τ_l = 4.0 × 10^{-7} s; 253 K, p_h = 0.38, τ_l = 5.0 × 10^{-7} s; 229 K, p_h = 0.24, τ_l = 7.4 × 10^{-7} s; 189 K, p_h = 0.10, τ_l = 1.4 × 10^{-5} s.

(f) Spin-Equilibrium Phenomena in Solution. The acetone solutions of these fast-spin-crossover complexes $[Fe(acpa)_2]BPh_4 \cdot H_2O$ and $[Fe(bzpa)_2]PF_6 \cdot 2H_2O$ show reversible thermochroism from violet (~300 K) to blue (~230 K) for $[Fe(acpa)_2]BPh_4 \cdot H_2O$ and from deep blue (~300 K) to bluish green (~230 K) for $[Fe(bzpa)_2]PF_6 \cdot H_2O$. The color change

(30) H. H. Wickman, "Mössbauer Effect Methodology", Vol. 2, I. J. Gruverman, Ed., Plenum Press, New York, 1966.

of the solution containing the complexes is usually interpreted in terms of a change of the electronic ground state of the complexes.

The electronic spectra were measured in the 300–1000-nm range for these complexes. A 550-nm band at 300 K is found to decrease steadily in intensity with decreasing temperature and is assigned to a high-spin state. Conversely a 700-nm band appears at low temperature (~230 K) and increases in intensity with decreasing temperature and is assigned to a low-spin state. These bands may be due to the metal–ligand charge transfer in origin because its absorption coefficients are about 10^4 l/(mol cm). The spin-state transition in solution is proceeded by the mechanism taking place in a molecule (intramolecular phenomenon). The existence of the bands due to the ^2T and ^6A states implies that the rate of the spin interconversion is slower than 10^{15} s^{-1} in solution. The rate of the spin interconversion in a solid state would be different from that in solution; however, these results would support the idea that the fast spin interconversion observed in the solid state proceeds fundamentally via an intramolecular mechanism (electronic factor) and also is influenced by the combined electron–phonon excitation.

Contribution from the Department of Chemistry,
Wayne State University, Detroit, Michigan 48202

Oxidation–Reduction Reactions of Complexes with Macrocyclic Ligands. Electron-Transfer Reactivity of a 1:1 Cobalt(II)–Dioxygen Adduct[1]

KRISHAN KUMAR and JOHN F. ENDICOTT*

Received June 15, 1983

The 1-equiv oxidation–reduction reactions of the transient 1:1 $Co^{II}(N_4)$–O_2 adduct, $Co([14]aneN_4)(OH_2)O_2^{2+}$ ([14]aneN$_4$ = 1,4,8,11-tetraazacyclotetradecane), have been examined. The kinetic behavior with outer-sphere reduction agents, combined with the kinetics of oxidation of $Co([14]aneN_4)(OH_2)O_2H^{2+}$ by $Ru(NH_3)_4phen^{3+}$, implies that $E^f \simeq 0.3 \pm 0.1$ V and $k_{exch} \simeq 10^{3\pm1}$ M^{-1} s^{-1} for the $Co([14]aneN_4)(OH_2)O_2^{2+,+}$ couple. Reactions of the $Co^{II}(N_4)O_2$ adduct with labile mildly reducing partners such as $Co^{II}(N_4)$ or $Fe(OH_2)_6^{2+}$ result in formation of μ-peroxo complexes. The rates of these "inner-sphere" reactions seem to be mostly a function of the equilibrium constant for adduct formation (k, M^{-1} s^{-1} (K, M^{-1})): 5×10^5 (8×10^5), 3.6×10^4 (10^4), 1.1×10^3 ($\leq 10^3$), respectively, for $Co([14]aneN_4)(OH_2)_2^{2+}$, $Co([15]aneN_4)(OH_2)_2^{2+}$, and $Fe(OH_2)_6^{2+}$. The adduct did not exhibit significant radical character, nor was it significantly basic ($pK_a < 0.1$ for $Co([14]aneN_4)(OH_2)O_2H^{3+}$).

Introduction

Reactions of dioxygen with organic and inorganic substrates are ubiquitous and of central importance in the chemistry of fuels, in aspects of synthesis, and in biological processes. Yet, molecular oxygen is notoriously sluggish in its reactions and often requires "activation", frequently by means of coordination in a transition-metal complex.[2] Neither the origins of the kinetic barriers to O_2 reactions nor the means of their relaxation by coordination is well understood.

Simple, one-electron-transfer reactions of dioxygen moieties have recently received some attention.[2d,3-5] The advantage of study of such simple reactions is that one can make use of the highly sophisticated understanding of electron-transfer chemistry[6-11] to gain insight into the reactivity patterns of dioxygen species. Unfortunately, the initial studies of such reactions have reached somewhat contradictory conclusions, with the large intrinsic barrier to electron transfer in the O_2–O_2^- couple being attributed largely to solvent reorganization,[3] while that of the (μ-superoxo)–(μ-peroxo) couples has been attributed to the change in O–O bond length.[4]

The 1:1 dioxygen–transition metal adducts tend to exist only as reactive intermediates, or transient species in aqueous solutions at room temperature. As a consequence, there have been very few studies that directly investigate the chemical behavior of such adducts. Owing to a fortuitous combination of formation constants and absorptivities, we have been able to find conditions for which the transient dioxygen adduct of $Co([14]aneN_4)(OH_2)_2^{2+}$[12] can be directly observed in reaction mixtures.[2d,13] Since the rate and equilibrium parameters in the O_2–$Co([14]aneN_4)(OH_2)_2^{2+}$ system have been fully characterized,[13] it is possible to systematically investigate the

(1) Partial support of this research by the National Institutes of Health (Grant AM 14341) is gratefully acknowledged.

(2) For general accounts see: (a) Hayaishi, O., Ed. "Molecular Mechanisms of Oxygen Activation"; Academic Press: New York, 1974. (b) Hayaishi, O., Ed. "Oxygenases"; Academic Press: New York, 1976. (c) Spiro, T. G., Ed. "Metal Ion Activation of Dioxygen"; Wiley: New York, 1980. (d) Endicott, J. F.; Kumar, K. *ACS Symp. Ser.* **1982**, *No. 198*, 425. (e) Basolo, F.; Hoffman, B. M.; Ibers, J. A. *Acc. Chem. Res.* **1976**, *9*, 175. (f) McLendon, G.; Martell, A. E. *Coord. Chem. Rev.* **1976**, *18*, 125. (g) Wilkins, R. G. *Adv. Chem. Ser.* **1971**, *No. 100*, 111. (h) Collman, J. P. *Acc. Chem. Res.* **1979**, *10*, 265. (i) Jones, R. D.; Summerville, D. A.; Basolo, F. *Chem. Rev.* **1979**, *79*, 140. (j) Martell, A. E. *Acc. Chem. Res.* **1982**, *15*, 155. (k) Sawyer, D. T.; Nanni, E. J.; Roberts, J. L., Jr. *Adv. Chem. Ser.* **1982**, *No. 201*, 585.

(3) (a) Stanbury, D. M.; Hass, O.; Taube, H. *Inorg. Chem.* **1980**, *19*, 518. (b) Stanbury, D. M.; Mulac, W. A.; Sullivan, J. C.; Taube, H. *Ibid.* **1980**, *19*, 3735.

(4) McLendon, G.; Mooney, W. F. *Inorg. Chem.* **1980**, *19*, 12.

(5) (a) Natarajan, P.; Raghavan, N. V. *J. Am. Chem. Soc.* **1980**, *101*, 4518. (b) Chandrasekaran, K.; Natarajan, P. *J. Chem. Soc., Dalton Trans.* **1981**, 478.

(6) (a) Marcus, R. A. *Discuss. Faraday Soc.* **1960**, *29*, 21. (b) *Annu. Rev. Phys. Chem.* **1964**, *15*, 155. (c) Marcus, R. A.; Siders, P. *ACS Symp. Ser.* **1982**, *No. 198*, 235.

(7) (a) Brunschwig, B. S.; Logan, J.; Newton, M. D.; Sutin, N. *J. Am. Chem. Soc.* **1980**, *102*, 5798. (b) Sutin, N.; Brunschwig, B. S. *ACS Symp. Ser.* **1982**, *No. 198*, 105. (c) Sutin, N. *Acc. Chem. Res.* **1982**, *15*, 275.

(8) (a) Newton, M. D. *Int. J. Quantum Chem.: Quantum Chem. Symp.* **1980**, *No. 14*, 363. (b) *ACS Symp. Ser.* **1982**, *No. 198*, 255.

(9) (a) Hush, N. S. *Trans. Faraday Soc.* **1961**, *57*, 155. (b) *Electrochim. Acta* **1961**, *57*, 155. (c) *ACS Symp. Ser.* **1982**, *No. 198*, 301.

(10) (a) Kestner, N. R.; Logan, J.; Jortner, J. *J. Phys. Chem.* **1974**, *78*, 2148. (b) Jortner, J. *J. Chem. Phys.* **1976**, *64*, 4860. (c) Buhks, E.; Bixon, M.; Jortner, J.; Navon, G. *Inorg. Chem.* **1979**, *18*, 2014.

(11) Endicott, J. F.; Kumar, K.; Ramasami, T.; Rotzinger, F. P. *Prog. Inorg. Chem.* **1983**, *30*, 141.

(12) Abbreviations: [14]aneN$_4$ = 1,4,8,11-tetraazacyclotetradecane; [15]aneN$_4$= 1,4,8,11-tetraazacyclopentadecane; Me$_4$[14]tetraeneN$_4$ = 2,3,9,10-tetramethyl-1,4,8,11-tetraazacyclotetradeca-1,3,8,10-tetraene; Me$_6$[14]4,11-dieneN$_4$ = 5,7,7,12,14,14-hexamethyl-1,4,8,11-tetraazacyclotetradeca-4,11-diene; sep = sepulchrate = (*S*)-1,3,6,8,10,13,16,19-octaazabicyclo[6.6.6]eicosane; phen = 1,10-phenanthroline.

0020-1669/84/1323-2447$01.50/0